ARTICLES
https://doi.org/10.1038/s41929-017-0004-2
nature catalysis

A bioinspired soluble manganese cluster as a water oxidation electrocatalyst with low overpotential

Galia Maayan[1,2*], Naama Gluz[1] and George Christou[2]

The electrocatalytic oxidation of water is a challenging step towards the production of hydrogen as an alternative fuel. In nature, water oxidation is catalysed by a high oxidation state Mn_4CaO_x cluster. The corresponding industrial development of manganese catalysts for water oxidation is very attractive due to the low cost of this metal. A few manganese complexes have been previously explored as water oxidation catalysts using various chemical oxidants in homogeneous and heterogeneous systems. Efficient electrochemical water oxidation catalysed by a soluble manganese-oxo cluster, however, has not been achieved. Here, we report the synthesis and characterization of $[Mn_{12}O_{12}(O_2CC_6H_3(OH)_2)_{16}(H_2O)_4]$ (Mn_{12}DH), a unique example within this class of compounds in being both highly soluble and stable in water. We demonstrate that Mn_{12}DH, which is readily prepared from cheap and environmentally benign starting materials, is a stable homogeneous water oxidation electrocatalyst operating at pH 6 with an exceptionally low overpotential of only 334 mV.

The catalytic splitting of water into hydrogen and oxygen is a bio-inspired challenge for chemists seeking to find renewable alternatives to fossil fuels. In nature, the oxygen-evolving complex (OEC) near photosystem II in green plants and cyanobacteria catalyses the oxidation of H_2O, employing solar energy to drive electron transfer[1,2]. This four-electron redox reaction (equations (1)–(3)) is a formidable process accomplished by a Mn_4CaO_x cluster[3,4]. A few synthetic Mn_xCaO_y clusters structurally similar to the OEC have been published[5–7], but catalytic water oxidation by these clusters has not been reported.

$$2H_2O \rightarrow O_2 + 4H^+ + 4e^-$$
$$E = 1.23\ \text{V} - 0.059\ \text{V} \times \text{pH (at 25 °C vs NHE)} \quad (1)$$

$$4H^+ + 4e^- \rightarrow 2H_2 \quad (2)$$

$$2H_2O \rightarrow O_2 + 2H_2 \quad (3)$$

Nevertheless, attempts over many years to emulate both the structure and function of the OEC have yielded various small Mn_x ($x \leq 4$) compounds[8], some of which catalyse water oxidation in heterogeneous[9–11] or homogeneous[12–15] systems[16,17]. The catalytic activity of these clusters, however, is hampered by their low stability either in water or under reaction conditions. Mn-based water oxidation catalysts typically utilize chemical oxidants such as peroxides, limiting the choice of catalysts to those that can structurally withstand such reactive reagents and often leading to uncertainties about the source of the obtained O_2 (ref. [18]). In order to avoid the latter, the oxidants Ce^{IV} and Ru^{III} have been employed in a few homogeneous[4,19,20] and heterogeneous[7] Mn-based catalytic systems, albeit with very low ($<2\,h^{-1}$) or no turnover number (TON)[19] and at high oxidant loading (for example, 480 equiv. of Ru^{III})[20]. Moreover, Ce^{IV} is only stable at low pH and Ru^{III} is a precious metal. Although water oxidation electrocatalysts containing metal ions[21] such as Ru (refs. [22,23]), Co (refs. [24–26]), Ir (ref. [27]), and Cu (refs. [28,29]) are undergoing extensive development, there is currently only one example of homogeneous electrocatalytic water oxidation by a Mn-based compound—a Mn porphyrin dimer reported more than twenty years ago. However, the highest activity—a turnover frequency (TOF) of $0.11\ \text{min}^{-1}$—was obtained in MeCN solution containing 5% v/v H_2O at a high potential of 2.0 V versus Ag/Ag^+ (2.58 V versus NHE) and in the presence of NBu^n_4OH (ref. [30]). Therefore, efficient homogeneous electrocatalysts for water oxidation based on water-soluble and -stable Mn clusters have yet to be developed.

It was previously suggested that the Mn^{IV}-O-Mn^{III}-H_2O motif (Fig. 1a, marked in pink) plays an important structural role in the activity of the OEC and its mimics[10,31]. Interestingly, this motif is a multiple structural element in the $[Mn_{12}O_{12}(O_2CR)_{16}(H_2O)_4]$ (Mn_{12}; R = Me, Et, Ph, and so on) clusters[32] (Fig. 1b) but there are only two examples of their use as oxidation catalysts[33,34]. Nevertheless, these Mn_{12} clusters were attractive to us as potential water oxidation electrocatalysts for several reasons. First, they have a structure that greatly resembles that of the OEC: their core consists of a $[Mn^{IV}_4O^{2-}_4]$ cube held by eight additional O^{2-} ions within a non-planar ring of eight Mn^{III} ions. Sixteen bridging carboxylate groups and four terminal water molecules complete the peripheral ligation. The eight outer Mn^{III} ions are divided by fourfold symmetry into two groups of four ions each, Mn2 and Mn3, the latter binds the labile water molecules. Second, Mn_{12} clusters display multiple one-electron redox processes, whose exact values can be tuned by the choice of carboxylate R group[32]. Finally, Mn_{12} clusters can be easily synthesized from readily available starting materials including $Mn(acetate)_2$, $KMnO_4$ and organic acids, under normal aerobic conditions at room temperature[32]. Overall, these unique biomimetic properties of Mn_{12} clusters, namely the presence of high oxidation state Mn and four water binding sites that could facilitate water oxidation catalysis, as well as their straightforward and environmentally

[1]Schulich Faculty of Chemistry, Technion - Israel Institute of Technology, Haifa, Israel. [2]Department of Chemistry, University of Florida, Gainesville, FL, USA. *e-mail: gm92@technion.ac.il

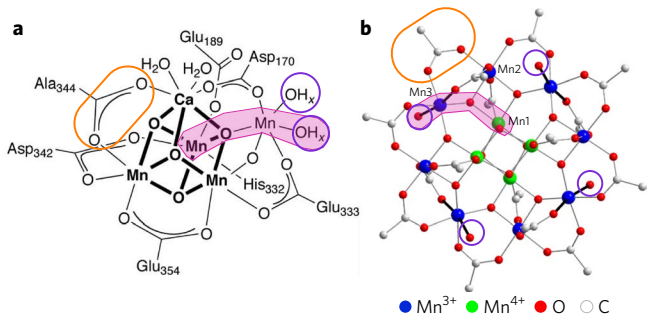

Fig. 1 | Mn_{12}Ac as a structural mimic of the OEC capable of reversible oxidation processes. a, The structure of the OEC and its surrounding peptide environment[6]. **b**, The structure of $[Mn_{12}O_{12}(O_2CMe)_{16}(H_2O)_4]$ (**Mn_{12}Ac**) viewed along the molecular *z* axis. Hydrogen atoms are omitted for clarity. The Mn^{IV}-O-Mn^{III}-H_2O motif is marked in pink, a representative carboxylate group is marked by an orange circle, and the labile water molecules are marked by a purple circle. Panel **a** adapted from ref. [6], AAAS.

benign synthesis from low-cost reagents, make them extremely attractive as potential catalysts for water oxidation. Unfortunately, almost all Mn_{12} complexes are insoluble in water, and those that do dissolve hydrolyse rapidly to insoluble Mn oxides and hydroxides. Consequently, the electrochemical performance of four Mn_{12} clusters deposited on tin oxide electrodes was recently examined. These clusters were shown to be heterogeneous electrocatalysts for water oxidation at natural pH with overpotentials of 640–820 mV (ref. [34]), but were also very unstable under the reaction conditions, and their decomposition was detected within one minute of electrolysis.

In this report, we describe how we have overcome this stability problem by using a ligand that is both bulky and hydrophilic, thereby providing access to a Mn_{12} derivative that is both soluble and stable in water. Electrochemical investigations allowed us to determine that it is an excellent homogeneous catalyst for water oxidation at an oxidation potential as low as 1.21 V (versus NHE). First, O_2 evolution was clearly detected by its reduction peak to superoxide observed in cyclic voltammograms. Second, controlled potential electrolysis and scan rate experiments indicate that this catalyst performs at pH 6 with high TON, high Faradic efficiency, and with low overpotential, establishing the Mn_{12} clusters, and by extension other high nuclearity Mn–oxo molecular clusters, as a viable new approach in this highly topical area.

Results

Synthesis and characterization of water-soluble Mn_{12}DH. It is known that **Mn_{12}Ac** is very soluble in water, but rapid hydrolysis occurs and gives a brown Mn oxide flocculent precipitate within seconds (Supplementary Fig. 1). In contrast, $[Mn_{12}O_{12}(O_2CPh)_{16}(H_2O)_4]$ (**Mn_{12}Bz**) is completely insoluble in water (Supplementary Fig. 2), as are almost all other Mn_{12} clusters. We therefore envisioned a compound that possesses bulky benzoate ligands to protect the core, but with at least two hydrophilic groups on each ligand to impart water solubility. In addition, the carboxylic acid moiety of this ligand should have a pK_a lower than that of $MeCO_2H$ (4.76), as the preparation of such a cluster would involve a carboxylate substitution[32] on **Mn_{12}Ac** driven to completion by the excess of the substituting acid and its greater acidity versus $MeCO_2H$. To meet these requirements, we chose 3,5-dihydroxybenzoic acid ($C_6H_3(OH)_2CO_2H$; dhbH), which is readily available, cheap and has a high water solubility of 51 g l^{-1} at 25 °C and a pK_a of 4.04 (for its acid group). $[Mn_{12}O_{12}(dhb)_{16}(H_2O)_4]$ (**Mn_{12}DH**) was prepared in one step by treatment of **Mn_{12}Ac** with 42 equiv. of dhbH in MeCN (equation (4)); **Mn_{12}Ac** is available in high yield from a one-step reaction of Mn^{II} acetate and $KMnO_4$ in aqueous acetic acid (Supplementary Methods)[35].

$$\left[Mn_{12}O_{12}(O_2CMe)_{16}(H_2O)_4\right] + 16\ dhbH \rightarrow \left[Mn_{12}O_{12}(dhb)_{16}(H_2O)_4\right] + 16\ MeCO_2H \quad (4)$$

The product **Mn_{12}DH**, which precipitated overnight from the reaction solution as a brown powder, was collected, washed and dried, and found to be very soluble in water giving a clear brown solution (Supplementary Fig. 3) that persists for long periods (months) with no flocculent precipitate. **Mn_{12}DH** was characterized by combustion analysis as well as in solution by Fourier-transform infrared spectroscopy (FT-IR), X-ray photoelectron spectroscopy (XPS) and UV/vis spectroscopy. The spectra were comparable with the corresponding characteristic spectra of **Mn_{12}Ac** and **Mn_{12}Bz** (ref. [36]). It was anticipated that the numerous polar –OH groups on the surface of **Mn_{12}DH** would lead to many hydrogen-bonded interstitial solvent molecules in the solid state, and indeed anlaysis indicated it as $[Mn_{12}O_{12}(O_2CC_6H_3(OH)_2)_{16}(H_2O)_4]\cdot 10H_2O\cdot 2MeCN$. The IR spectrum of **$Mn_{12}$DH** is very similar to that of **Mn_{12}Bz** but with three differences: (i) the broad absorbance band at $\nu = 3{,}300$ cm^{-1} assignable to O–H stretching modes is much stronger, due to the additional H_2O content; (ii) the carboxylate bands are broader, due to the extensive hydrogen-bonding they are involved in; and (iii) there is a new band at $\nu = 856$ cm^{-1} assignable (on the basis of the free dhbH spectrum) to the hydroxy-Ph ring (Supplementary Fig. 4). IR spectra were also employed to probe the stability of **Mn_{12}DH** in water: an aqueous solution of **Mn_{12}DH** was maintained at room temperature for three days, and then the solid re-isolated by freeze-drying. The IR spectrum of this solid was identical to that before dissolution (Supplementary Fig. 4), confirming no hydrolysis. These IR spectra are consistent with **Mn_{12}DH** retaining the $[Mn_{12}O_{12}(O_2CR)_{16}(H_2O)_4]$ structure. This was further supported by the **Mn_{12}DH** XPS spectrum, which is similar to that of **Mn_{12}Ac** (ref. [36]), exhibiting two typical Mn–O peaks (Supplementary Fig. 5). Additionally, the UV/vis spectrum of **Mn_{12}DH** in water shows two absorption bands near 240 and 300 nm, which are shifted about 10 nm relative to dhbH and can be assigned to the dhb^- ligands (Supplementary Fig. 6). Overall, the combined data confirm that **Mn_{12}DH** is a new member of the Mn_{12} family.

Cyclic voltammetry experiments. The oxidation of **Mn_{12}Ac** was investigated by cyclic voltammetry (CV) in dry MeCN in an inert-atmosphere glove box (Fig. 2a). This CV exhibits four reversible one-electron processes, two oxidations at $E_f/E_r = 1.18/1.06$ and 1.44/1.27 V, and two reductions at 0.23/0.35 and 0.49/0.56 V (versus NHE) — E_f and E_r are the E_p peak potentials for the forward (f) and reverse (r) scans of each redox process. Previous studies of the reduction processes of various Mn_{12} clusters have confirmed their one-electron nature by isolation of $[Mn_{12}]^{n-}$ ($n = 1$–3) salts, including crystallographic characterization of $n = 1$ and 2 examples, which also showed reduction of the Mn3 ions to Mn^{II} (ref. [32]). Extension to the oxidations shown in Fig. 2a confirms that these are also one-electron processes, assigned to the oxidation of Mn^{III} to Mn^{IV} (equation (5)).

$$[Mn_8^{III}Mn_4^{IV}] \rightarrow [Mn_7^{III}Mn_5^{IV}]^+ \rightarrow [Mn_6^{III}Mn_6^{IV}]^{2+} \quad (5)$$

The electrochemistry of **Mn_{12}DH** was explored in aqueous acetate buffer at pH 6.0, the prevailing pH at the OEC, in which **Mn_{12}DH** was found to be stable for long periods and which is often used for water oxidation studies of dinuclear Mn_2 clusters[37,38]. The CV of **Mn_{12}DH** in this medium, scanning initially in the anodic direction, shows two oxidation waves at $E_p = 0.95$ and 1.6 V versus NHE and two cathodic peaks at $E_p = 0.8$ (small) and −0.45 V

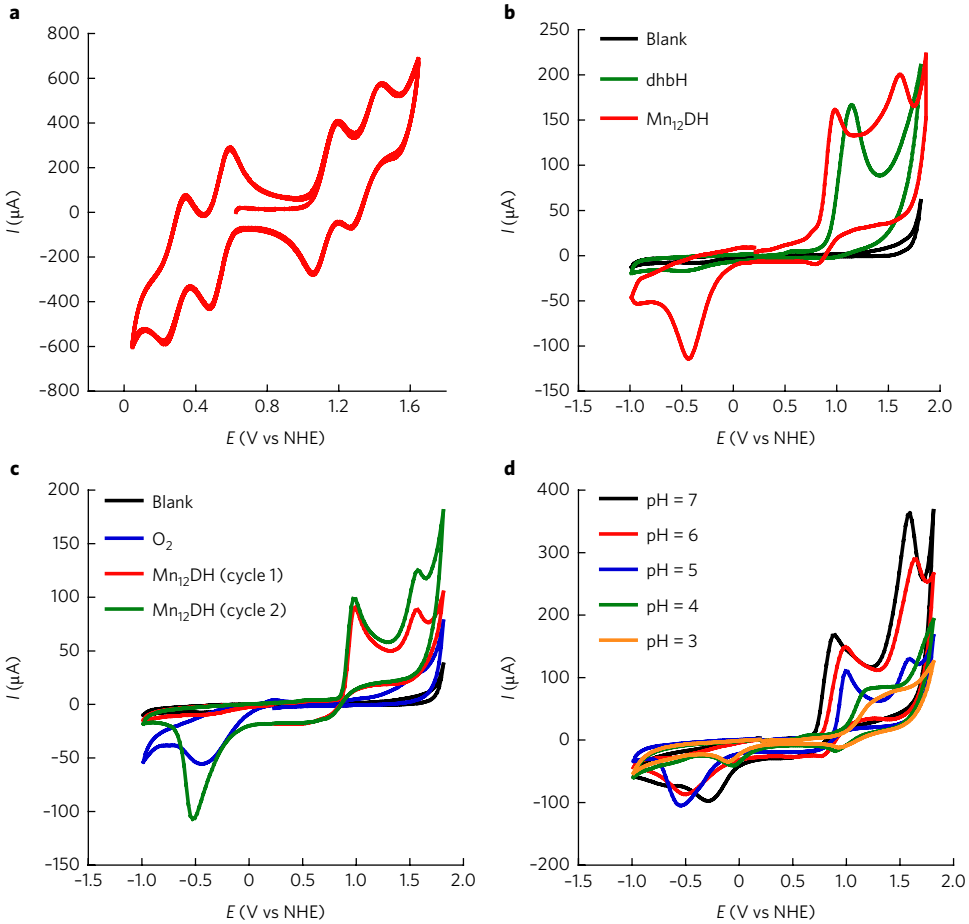

Fig. 2 | Cyclic voltammograms. a, **Mn_{12}Ac** (1.74 mM) in dry deoxygenated MeCN in an inert-atmosphere glove box, showing four consecutive cycles at 10 mV s^{-1} scanning initially from 0.5 V in the positive direction. **b**, Deoxygenated 0.1 M acetate buffer at pH 6.0 (black); 0.1 M acetate buffer at pH 6.0 containing 0.5 mM **Mn_{12}DH** (red); deoxygenated 0.1 M acetate buffer at pH 6.0 containing 8 mM dhbH (green). All initial CV scans were in the anodic direction at 100 mV s^{-1}. **c**, 0.1 M acetate buffer at pH 6.0 (black); after bubbling O_2 through for 1 min (blue); deoxygenated 0.1 M acetate buffer at pH 6.0 containing 0.5 mM **Mn_{12}DH** (red and green). All the initial CV scans were in the cathodic direction at 100 mV s^{-1}. **d**, Deoxygenated 0.1 M acetate buffer at pH 7.0 containing 0.5 mM **Mn_{12}DH** (black); at pH 6.0 (red); at pH 5.0 (blue); at pH 4 (green) and at pH 3 (orange). The potential was measured versus the Ag/AgCl reference electrode and converted to versus NHE by using E (NHE) = E (Ag/AgCl) + 0.21 V. Deoxygenation was accomplished by bubbling N_2 through the solutions for 5 min.

(intense, Fig. 2b, red line); under the same conditions, dhbH exhibited an oxidation peak at 1.15 V versus NHE, and a very small reduction peak at −0.45 V (Fig. 2b, green line). Interestingly, when the scan direction for **Mn_{12}DH** was reversed, the −0.45 V feature was absent in the first cycle (Fig. 2c, red line) but appeared again in the following cycle (Fig. 2c, green line), indicating that it arises from the high potential oxidation processes. A control solution of acetate buffer at pH 6.0 saturated with O_2 and containing no **Mn_{12}DH** identified the −0.45 V feature as the reduction of O_2 to superoxide (Fig. 2b, blue line). The CV scans thus indicate that the oxidation of **Mn_{12}DH** triggers electrocatalytic water oxidation to O_2. The small cathodic wave at E_p = 0.8 V corresponds to the re-reduction of remaining oxidized cluster back to its resting state **Mn_{12}DH**; continuous CV scans over four cycles showed essentially superimposable profiles (Supplementary Fig. 7), supporting the high stability of **Mn_{12}DH** under these conditions. The irreversible oxidation wave of free dhbH at 1.15 V shows significant decay of its intensity over four scans (Supplementary Fig. 8), suggesting a non-reversible oxidation of at least one hydroxyl group. As this decay is absent from the continuous CV scans of **Mn_{12}DH** we can assume that the hydroxyl groups do not get oxidized at this potential range.

On the basis of these measurements, an important follow-up question was which oxidation event was triggering the water oxidation. To answer this, the CV scans were switched (reversed) at various potentials in the 0.71 to 1.81 V range (Fig. 3), and an interesting trend was observed. As the switching potential decreases from 1.81 V (Fig. 3a), the height of the reverse peak on the first oxidation increases and the amount of O_2 generated decreases (as gauged by the size of the O_2 reduction wave), becoming essentially constant for switching potentials after the first oxidation but before the second, that is, 1.21–1.41 V. Decreasing the switching potential at or below 1.21 V (Fig. 3b) has little effect on the O_2 evolved until it is switched at 0.91 V, which causes a significant decrease in the amount of O_2. Switching at 0.81 or 0.71 V gives only traces of O_2. We conclude that scanning through both oxidation processes leads to a more-efficient water oxidation electrocatalyst, but that the first oxidation alone is enough to yield O_2. The CV study thus provides strong evidence that **Mn_{12}DH** is an excellent catalyst for the electrochemical oxidation of water to O_2, and at a low overpotential—the thermodynamic potential for water oxidation at pH 6.0 at 25 °C is 0.88 V versus NHE, while we already observe significant oxygen evolution by 1.0 V. We suspect that the increased evolution of O_2 on scanning past the second oxidation is due to water oxidation catalysis now

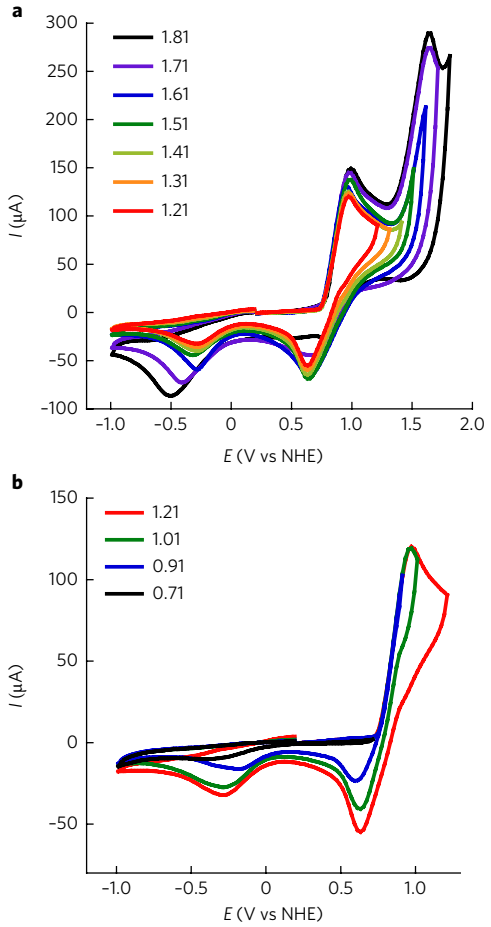

Fig. 3 | Cyclic voltammograms at 100 mV s^{-1} for Mn_{12}DH in deoxygenated 0.1 M acetate buffer at pH 6.0. a, The anodic scans were reversed at 1.21 V (red), 1.31 V (orange), 1.41 V (light green), 1.51 V (green), 1.61 V (blue), 1.71 V (purple) and 1.81 V (black) versus NHE. **b**, The anodic scans were reversed at 0.71 V (black), 0.91 V (blue), 1.01 V (green) and 1.21 V (red) versus NHE. All scans were initially in the anodic direction.

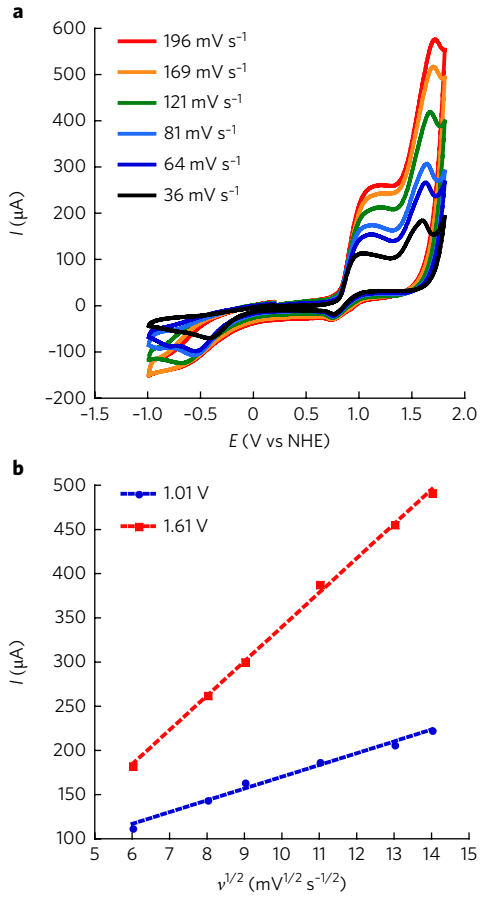

Fig. 4 | Scan rate dependence experiments. a, CV of **Mn_{12}DH** at different scan rates in 0.1 M acetate buffer at pH 6. **b**, The relation between the catalytic current of **Mn_{12}DH** and the square root of the scan rate.

taking place at multiple sites on the **Mn_{12}DH** molecule, consistent with the multiple water binding sites in the structure; however, the multiple sites within such an oxide-bridged cluster are not necessarily completely independent of each other. This would rationalize the fact that scanning only through the first oxidation still gives significant O_2 evolution. If two-electron oxidation was required to trigger water oxidation, then O_2 generation would not be expected to be significant on switching after only the first oxidation.

The pH dependence of the electrochemical behaviour of **Mn_{12}DH** was investigated by CV scans in acetate buffer in the pH 3.0–7.0 range (Fig. 2d). Significant catalytic currents as well as oxygen evolution, indicated by the oxygen reduction peak, were only observed at pH values of 5, 6 and 7. The E_p values for the catalytic water oxidation peak current decrease slightly as the pH increases and the most-intense catalytic peaks were obtained at pH 6 and 7. These observations are consistent with the water oxidation process, which is kinetically not favoured in acidic solution.

Catalyst stability. In order to exclude the possibility of electrodeposition of decomposition products on the electrode, and confirm that the catalytic process is homogeneous, we explored whether a manganese oxide film was being formed on the surface of the electrode. To do so, we removed the glassy carbon electrode from a solution of **Mn_{12}DH** (0.5 mM in 0.1 M acetate buffer, pH 6) after carrying out 25 continuous CV scans from −1.0 V to 1.81 V versus NHE, rinsed it with water (the electrode was not polished), and placed it in fresh 0.1 M acetate buffer solution at pH 6 containing no **Mn_{12}DH**. The CV scan of this solution showed no oxidation peaks and was the same as the CV scan of the blank solution in Fig. 2b (Supplementary Fig. 9). In addition, we examined the scan rate dependence of the **Mn_{12}DH** oxidation currents in 0.1 M acetate buffer at pH 6 (Fig. 4a). A linear fit was obtained when the intensity at the peak of each oxidation event was plotted against the square root of the scan rate (Fig. 4b), confirming that the oxidation currents are diffusion controlled and the catalytic process is truly homogeneous[39].

Bulk electrolysis experiments and kinetic data. As oxygen evolution was observed at the low potential of 1.01 V and in order to assess the efficacy of **Mn_{12}DH** at a low overpotential, controlled potential electrolysis (CPE) experiments were initially carried out for 30 min in a double-compartment cell at pH 6 and an applied potential of either 1.01 V or 1.21 V versus NHE (Supplementary Fig. 10). In these conditions, oxygen evolution was detected only when a potential of 1.21 V was applied. Thus, we conducted a five-hour CPE experiment at 1.21 V with 2.5 μmol **Mn_{12}DH** (Fig. 5a, red line), which afforded charge accumulation of 43.8 C whereas a control experiment run under identical conditions, but without the catalyst (blank, Fig. 5a, black line), showed a charge accumulation of only 2.2 C. A CPE experiment conducted under the same conditions with 40 μmol of dhbH (this was calculated based on

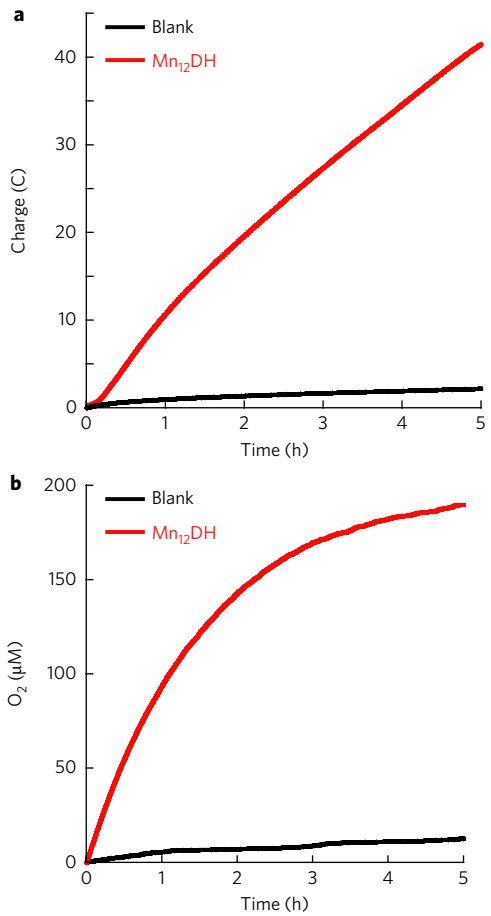

Fig. 5 | Bulk electrolysis and direct oxygen measurements. a,**b**, Electrolysis data showing charge passed versus time (**a**) and molecular oxygen values as measured during CPE showing oxygen evolution versus time (**b**), for a 5 ml solution containing 2.5 μmol of **Mn_{12}DH** in 0.1 M acetate buffer at pH 6 (red lines), and data for the buffer solution alone (black lines), with the cell operating at a potential of 1.21 V versus NHE.

2.5 μmol, which is the amount of used cluster, multiplied by 16, as there are 16 ligand molecules per cluster molecule; Supplementary Fig. 11) afforded charge accumulation similar to the blank solution, indicating that the catalyst for O_2 evolution is **Mn_{12}DH**.

Direct O_2 measurements were carried out during the CPE experiment using an optical fibre oxygen meter probing the headspace of the solution. Accordingly, about 190 μM oxygen was evolved over 5 h with **Mn_{12}DH** and only 13 μM without it (Fig. 5b). These results translated to a total of 38.1 μmol of evolved oxygen, representing a TON of about 15.5 in 5 h based on 2.5 μmol of catalyst in the bulk solution. An additional way to calculate the TON of this reaction is based on the apparent rate constant of the reaction, k_{obs}, which could be obtained from a foot-of-the-wave analysis (FOWA)[40,41]. Following the literature[40,42], we performed FOWA from the data presented in Fig. 4a and found an average k_{obs} of 0.035 s^{-1}, and calculated a TON of 629 in 5 h (Supplementary Figs. 12,13, Supplementary Equations 1,2 and Supplementary Table 1).

Catalyst efficiency. As the catalysis slows down over the period of 5 h, it is convenient to calculate the Faradic efficiency based on the initial rate of the process. Accordingly, the Faradic efficiency in the first 20 min was calculated to be 77.9%. This Faradic efficiency, together with the observation that about 91% of the measured O_2 is being evolved in the first 3 h, suggests that another product, in addition to O_2, is being generated during the catalytic process. This might be CO_2, which could evolve due to catalyst decomposition. UV/vis spectra of **Mn_{12}DH** before and after 5 h bulk electrolysis at 1.21 V versus NHE show that the spectral intensity after bulk electrolysis decreased slightly but the two absorption bands remain intact and there is no evidence for the formation of new peaks (Supplementary Fig. 14). In addition, CV scans before and after 5 h bulk electrolysis show that both oxidation peaks as well as the oxygen reduction peak are maintained, but there is a decrease in the intensity of all three peaks (Supplementary Fig. 15). Both the UV/vis and CV results indicate a decrease in the overall concentration of **Mn_{12}DH**, which might be attributed to some degree of catalyst decomposition. These results are consistent with the Faradic efficiency and with the decrease in catalytic activity over time. Nevertheless, it is evident that some of the catalyst is still present in solution even after 5 h of CPE, demonstrating its stability relative to other similar catalysts[34]. This is efficient electrochemical water oxidation by a manganese cluster in a homogeneous catalytic system, and moreover, this electrocatalyst performs with a low overpotential of only 334 mV.

Discussion

One reason for the unique electrocatalytic activity of **Mn_{12}DH** might be related to its high nuclearity. Mn_{12} clusters are distinctly different from other catalysts studied in this area in that they are high nuclearity, homometallic molecular clusters that are intermediate between small molecules and bulk metal oxides. In addition, their multiple water-binding sites, twelve intimately associated Mn ions, and multiple reversible redox processes offer the possibility of homogeneous water oxidation catalysis at multiple surface sites with a core that could function as a charge reservoir to facilitate the multi-electron transformations involved. A second reason might be related to the hydroxyl substituents on the dhb^- ligands. It is possible that the hydroxyl groups contribute more to the catalysis than just ensuring the aqueous solubility and stability of **Mn_{12}DH**, by allowing the ligands to provide multiple shuttle pathways through hydrogen bonding, helping to bring H_2O molecules to the Mn ions in one direction and in the other direction removing H^+ ions generated from H_2O oxidation. Further studies are necessary to probe the exact role of the number and positions of hydroxyl or other hydrogen-bonding substituents on the electrocatalytic activity.

In conclusion, we have demonstrated the initial use of a high nuclearity Mn_{12}–oxo cluster as an efficient water oxidation electrocatalyst at low overpotential and in homogeneous solution. The use of Mn and readily available carboxylate ligands makes this result particularly pertinent to the search for efficient, cheap and environmentally benign catalysts that are highly active and robust in aqueous media. Via a simple carboxylate substitution, the bulky dhb^- ligands not only impart both water solubility and stability, but also probably assist the catalytic process by serving as hydrogen-bonding sites to provide H_2O and H^+ shuttle pathways to and from the catalytic Mn sites. The dhb^- ligands can thus be described as mimicking the polypeptide around the hydrolytically unstable Mn/Ca–oxo cluster of the OEC. **Mn_{12}DH** is a molecular cluster, which is significant because its properties can be tuned in a controlled manner, allowing future improvements in catalyst stability and activity. One possibility is adjusting the ligation environment and hydrogen-bonding properties by using hydroxy-benzoic acids differing in either the position of the hydroxy group(s) and/or their number. Ongoing efforts are also focusing on the use of other water-solubilizing carboxylate ligands for the generation of Mn_{12} clusters, as well as smaller nuclearity, high oxidation state Mn and Mn/Ca complexes to further facilitate charge- and light-driven catalytic processes relevant to sustainable energy.

Methods

Electrochemical methods. Cyclic voltammograms (CV) were conducted in a standard three-electrode cell assembly consisting of a glassy carbon electrode as the working electrode, Pt mesh as the counter (auxiliary) electrode, and a Ag/AgCl/3 M KCl reference electrode (+210 mV versus NHE). The CVs were typically recorded at a scan rate of 100 mV s^{-1}; E_{step} of 20/50 mV and sensitivity of 0.1 mA V^{-1} in acetate buffer pH 6 containing 0.5 mM **Mn_{12}DH**. No IR compensation was employed. Quoted potentials are versus NHE by the addition of 210 mV to the electrode values. In typical experiments, a stream of N_2 gas at atmospheric pressure was bubbled into the solution for 5 min prior to scanning. Controlled potential electrolysis experiments were performed in a three-compartment 'H–cell' separated by a medium-porosity sintered glass frit. Three-electrode assembly was used consisting of vitreous carbon-3000C Foam as the working electrode, Pt mesh as the counter (auxiliary) electrode, and a Ag/AgCl/3 M KCl reference electrode (+210 mV versus NHE). Only the side equipped with working and reference electrodes was loaded with the catalyst (typically 2.5 µmol). In typical experiments, a stream of Ar gas at atmospheric pressure was bubbled into the cell for 30 min prior to scanning.

Oxygen measurements. Direct oxygen measurements during bulk electrolysis were conducted using an optic fibre sensor housed inside the needle of a syringe. The needle is inserted into the cell at the anode compartment, and the evolved oxygen is measured at the headspace of the cell. The instrument displays the oxygen levels in µM, and in order to know the absolute amount of oxygen produced, in µmol, a calibration of the instrument was performed.

The synthesis and characterization of **Mn_{12}DH** are detailed in the Supplementary Methods.

Data availability. The data that support the plots within this paper and other findings of this study are available from the corresponding author upon reasonable request.

Received: 11 July 2017; Accepted: 18 October 2017;
Published online: 20 November 2017

References

1. Barber, J. Biological solar energy. *Philos. Trans. R. Soc. London Ser. A* **365**, 1007–1023 (2007).
2. Dau, H. & Zaharieva, I. Principles, efficiency, and blueprint character of solar-energy conversion in photosynthetic water oxidation. *Acc. Chem. Res.* **42**, 1861–1870 (2009).
3. Ferreira, K. N., Iverson, T. M., Maghlaoui, K., Barber, J. & Iwata, S. Architecture of the photosynthetic oxygen-evolving center. *Science* **303**, 1831–1838 (2004).
4. Umena, Y., Kawakami, K., Shen, J. R. & Kamiya, N. Crystal structure of oxygen-evolving photosystem II at a resolution of 1.9Å. *Nature* **473**, 55–60 (2011).
5. Zhang, C. et al. A synthetic Mn_4Ca-cluster mimicking the oxygen-evolving center of photosynthesis. *Science* **348**, 690–693 (2010).
6. Kanady, J. S., Tsui, E. Y., Day, M. W. & Agapie, T. A Synthetic model of the Mn_3Ca subsite of the oxygen-evolving complex in photosystem II. *Science* **333**, 733–736 (2011).
7. Mukherjee, S. et al. Synthetic model of the asymmetric $[Mn_3CaO_4]$ cubane core of the oxygen-evolving complex of photosystem II. *Proc. Natl Acad. Sci. USA* **109**, 2257–2262 (2012).
8. Manchanda, R., Brudvig, G. W. & Crabtree, R. H. High-valent oxomanganese clusters: structural and mechanistic work relevant to the oxygen-evolving center in photosystem II. *Coord. Chem. Rev.* **144**, 1–38 (1995).
9. Limburg, J. et al. A functional model for O–O bond formation by the O_2-evolving complex in photosystem II. *Science* **283**, 1524–1527 (1999).
10. Poulsen, A. K., Rompel, A. & McKenzie, C. J. Water oxidation catalyzed by a dinuclear Mn complex: a functional model for the oxygen-evolving center of photosystem II. *Angew. Chem. Int. Ed.* **44**, 6916–6920 (2005).
11. Tagore, R., Crabtree, R. H. & Brudvig, G. W. Oxygen evolution catalysis by a dimanganese complex and its relation to photosynthetic water oxidation. *Inorg. Chem.* **47**, 1815–1823 (2008).
12. Dismukes, G. C. et al. Development of bioinspired Mn_4O_4-cubane water oxidation catalysts: lessons from photosynthesis. *Acc. Chem. Res.* **42**, 1935–1943 (2009).
13. Najafpour, M. M., Ehrenberg, T., Wiechen, M. & Kurz, P. Calcium manganese(III) oxides ($CaMn_2O_4{\cdot}xH_2O$) as biomimetic oxygen-evolving catalysts. *Angew. Chem. Int. Ed.* **49**, 2233–2237 (2010).
14. Yagi, M., Toda, M., Yamada, S. & Yamazaki, H. An artificial model of photosynthetic photosystem II: visible-light-derived O_2 production from water by a di-µ-oxo-bridged manganese dimer as an oxygen evolving center. *Chem. Commun.* **46**, 8594–8596 (2010).
15. Brimblecombe, R., Koo, A., Dismukes, G. C., Swiegers, G. F. & Spiccia, L. Solar driven water oxidation by a bioinspired manganese molecular catalyst. *J. Am. Chem. Soc.* **132**, 2892–2894 (2010).
16. Rüttinger, W. & Dismukes, G. C. Synthetic water-oxidation catalysts for artificial photosynthetic water oxidation. *Chem. Rev.* **97**, 1–24 (1997).
17. Yagi, M. & Kaneko, M. Molecular catalysts for water oxidation. *Chem. Rev.* **101**, 21–35 (2001).
18. Kärkäs, M. D., Verho, O., Johnston, E. V. & Åkermark, B. Artificial photosynthesis: molecular systems for catalytic water oxidation. *Chem. Rev.* **114**, 11863–12001 (2014).
19. Tagore, R., Chen, H., Zhang, H., Crabtree, R. H. & Brudvig, G. W. Homogeneous water oxidation by a di-µ-oxo dimanganese complex in the presence of Ce^{4+}. *Inorg. Chim. Acta* **360**, 2983–2989 (2007).
20. Karlsson, E. A. et al. Photosensitized water oxidation by use of a bioinspired manganese catalyst. *Angew. Chem. Int. Ed.* **50**, 11715–11718 (2011).
21. Sala, X., Romero, I., Rodríguez, M., Escriche, L. & Llobet, A. Molecular catalysts that oxidize water to dioxygen. *Angew. Chem. Int. Ed.* **48**, 2842–2852 (2009).
22. Concepcion, J. J. et al. Making oxygen with ruthenium complexes. *Acc. Chem. Res.* **42**, 1954–1965 (2009).
23. Matheu, R. et al. Intramolecular proton transfer boosts water oxidation catalyzed by a Ru complex. *J. Am. Chem. Soc.* **137**, 10786–10795 (2015).
24. Kanan, M. W. & Nocera, D. G. *In situ* formation of an oxygen-evolving catalyst in neutral water containing phosphate and Co^{2+}. *Science* **321**, 1072–1075 (2008).
25. Jiao, F. & Frei, H. Nanostructured cobalt oxide clusters in mesoporous silica as efficient oxygen-evolving catalysts. *Angew. Chem. Int. Ed.* **48**, 1841–1844 (2009).
26. Yin, Q. et al. A fast soluble carbon-free molecular water oxidation catalyst based on abundant metals. *Science* **328**, 342–328 (2010).
27. Youngblood, W. J. et al. Photoassisted overall water splitting in a visible light-absorbing dye-sensitized photoelectrochemical cell. *J. Am. Chem. Soc.* **131**, 926–927 (2009).
28. Barnett, S. M., Goldberg, K. I. & Mayer, J. M. A soluble copper–bipyridine water-oxidation electrocatalyst. *Nat. Chem.* **4**, 498–502 (2012).
29. Zhang, M. T., Chen, Z., Kang, P. & Meyer, T. J. Electrocatalytic water oxidation with a copper(II) polypeptide complex. *J. Am. Chem. Soc.* **135**, 2048–2051 (2013).
30. Naruta, Y., Sasayama, M. A. & Sasaki, T. Oxygen evolution by oxidation of water with manganese porphyrin dimers. *Angew. Chem. Int. Ed.* **33**, 1839–1841 (1994).
31. Kärkäs, M. D. & Åkermark, B. Water oxidation using earth-abundant transition metal catalysts: opportunities and challenges. *Dalton Trans.* **45**, 14421–14461 (2016).
32. Bagai, R. & Christou, G. The *Drosophila* of single-molecule magnetism: $[Mn_{12}O_{12}(O_2CR)_{16}(H_2O)_4]$. *Chem. Soc. Rev.* **38**, 1011–1026 (2009).
33. Maayan, G. & Christou, G. 'Old' clusters with new function: oxidation catalysis by high oxidation state manganese and cerium/manganese clusters using O_2 gas. *Inorg. Chem.* **50**, 7015–7021 (2011).
34. Yan, Y., Lee, J. S. & Ruddy, D. A. Structure–function relationships for electrocatalytic water oxidation by molecular $[Mn_{12}O_{12}]$ clusters. *Inorg. Chem.* **54**, 4550–4555 (2015).
35. Sessoli, R. et al. High-spin molecules: $[Mn_{12}O_{12}(O_2CR)_{16}(H_2O)_4]$. *J. Am. Chem. Soc.* **115**, 1804–1816 (1993).
36. Means, J. et al. Films of Mn_{12}-acetate deposited by low-energy laser ablation. *J. Magn. Magn. Mater.* **284**, 215–219 (2004).
37. Limburg, J., Brudvig, G. W. & Crabtree, R. H. O_2 evolution and permanganate formation from high-valent manganese complexes. *J. Am. Chem. Soc.* **119**, 2761–2762 (1997).
38. Cady, C. W., Shinopoulos, K. E., Crabtree, R. H. & Brudvig, G. W. $[(H_2O)(terpy)Mn(\mu\text{-}O)_2Mn(terpy)(OH_2)](NO_3)_3$ (terpy = 2,2′:6,2′′-terpyridine) and its relevance to the oxygen-evolving complex of photosystem II examined through pH dependent cyclic voltammetry. *Dalton Trans.* **39**, 3985–3989 (2010).
39. Bard, A. J. & Faulkner, L. R. *Electrochemical Methods: Fundamentals and Applications* (Wiley, New York, 2001).
40. Costentin, C., Passard, G. & Savéant, J.-M. Benchmarking of homogeneous electrocatalysts: overpotential, turnover frequency, limiting turnover number. *J. Am. Chem. Soc.* **137**, 5461–5467 (2015).
41. Zhang, T., Wang, C., Liu, S., Wang, J. L. & Lin, W. A biomimetic copper water oxidation catalyst with low overpotential. *J. Am. Chem. Soc.* **136**, 273–281 (2014).
42. Garrido-Barros, P. et al. Redox non-innocent ligand controls water oxidation overpotential in a new family of mononuclear Cu-based efficient catalysts. *J. Am. Chem. Soc.* **137**, 6758–6761 (2015).

Acknowledgements

This research was funded by the Solar Fuels Israel Center of Research Excellence (I-CORE) of the Israeli Science Foundation (ISF), grant number 2018762, and

supported by the Grand Energy Technion Program. It was also funded by the USA National Science Foundation under grant CHE-1410394. We thank C. di Giovanni for the CV measurements of $\mathbf{Mn_{12}Ac}$ in the glove box and for Fig. 2a. G.M. is grateful to A. Llobet at ICIQ, Tarragona, Spain, for the opportunity to work in his laboratories in order to study oxygen measurement techniques and gain additional knowledge in electrochemistry.

Author contributions

G.M. and G.C. planned the research, and G.M. and N.G. performed the experiments. G.M., N.G. and G.C. prepared the manuscript.

Competing interests

The authors declare no competing financial interests.

Additional information

Supplementary information is available for this paper at https://doi.org/10.1038/s41929-017-0004-2.

Reprints and permissions information is available at www.nature.com/reprints.

Correspondence and requests for materials should be addressed to G.M.

Publisher's note: Springer Nature remains neutral with regard to jurisdictional claims in published maps and institutional affiliations.